Filtenna-Filter-Filtenna-Based FSS With Simultaneous Wide Passband and Wide Out-of-Band Rejection Using Multiple-Mode Resonators

Huawei Lin, Sai-Wai Wong, *Senior Member, IEEE*, Kam-Weng Tam, *Senior Member, IEEE*, Yin Li, Kong Ngai, Chi-Hou Chio, *Member, IEEE*, and Yejun He, *Senior Member, IEEE*

***Abstract*— A novel filtenna-filter-filtenna (FA-F-FA)-based frequency-selective surface (FSS) technique is proposed using multiple-mode resonators (MMRs). Based on this method, a bandpass FSS with simultaneous wide passband and wide out-of-band rejection is validated. The MMR unit cell consists of two back-to-back magnetoelectric (ME)-dipole antennas and a filter-embedded GND plane. Four modes are analyzed and used to acquire a wide passband of the FSS. At the same time, wide out-of-band rejections in both lower and upper bands are controlled by the filter-embedded GND plane with four rotationally symmetric quarter-wavelength transmission lines (QWTLs). Moreover, the GND plane plays a crucial role in the impedance matching of the proposed FSS. As a result, four transmission poles (TPs) and three transmission zeros (TZs) of the proposed FSS can be obtained, leading to a fourth-order filtering response and wide out-of-band rejection. An equivalent circuit model, current distributions, and electric field distributions are introduced to illustrate the working mechanism of the FSS. Finally, the proposed FA-F-FA-based FSS with a 50.2% 3-dB fractional bandwidth (FBW_{3dB}) in the passband and 53.5% and 119.2% of the 20-dB fractional bandwidth (FBW_{20dB}), respectively, in the lower and upper rejection bands is achieved. The S-parameters are stable under an oblique incident angle of 50°. The measured and simulated results are in good agreement. In addition, the proposed FSS has the advantages of low profile, assembly free, and dual-polarization application, which verify the versatility of the FA-F-FA-based MMR FSS.**

***Index Terms*— Filtenna, filter, frequency-selective surface (FSS), magnetoelectric (ME)-dipole antenna, multiple-mode resonators (MMRs), wide out-of-band rejection, wide passband.**

Manuscript received 1 December 2022; revised 21 February 2023; accepted 16 March 2023. Date of publication 7 April 2023; date of current version 2 June 2023. This work was supported in part by the National Natural Science Foundation of China under Grant 62171289, in part by the Shenzhen Science and Technology Programs under Grant JCYJ 20190728151457763 and Grant JCYJ 20200109113601723, and in part by the Macao Science and Technology Development Fund under Grant FDCT 0013/2021/AGJ. *(Corresponding author: Sai-Wai Wong.)*

Huawei Lin, Kam-Weng Tam, and Chi-Hou Chio are with the Faculty of Science and Technology, University of Macau, Macau, SAR, China (e-mail: yc17440@umac.mo; kentam@umac.mo; yb57422@um.edu.mo).

Sai-Wai Wong and Yejun He are with the College of Electronics and Information Engineering, Shenzhen University, Shenzhen 518060, China (e-mail: wongsaiwai@ieee.org; heyejun@126.com).

Yin Li is with the Peng Cheng Laboratory, Shenzhen 518066, China (e-mail: liy17@pcl.ac.cn).

Kong Ngai is with Crosstech Innovation Group Ltd., Macau, SAR, China (e-mail: nkong@crosstech.group).

Color versions of one or more figures in this article are available at https://doi.org/10.1109/TAP.2023.3263895.

Digital Object Identifier 10.1109/TAP.2023.3263895

I. Introduction

FREQUENCY-SELECTIVE surfaces (FSSs) comprised of periodic structures can manipulate electromagnetic waves, exhibiting bandpass or bandstop response. Therefore, different FSSs have been widely used in antenna radomes, dichroic subreflectors, electromagnetic shelters, and so on [1], [2], [3]. In these applications, an ideal bandpass filtering response for incident electromagnetic waves is desired, where low profile, high selectivity, low in-band loss, high out-of-band rejection, and angular stability should be the figure of merit realized. In addition, FSSs with wide passband and wide out-of-rejection bands are gradually substantial in wideband transmitarray [4], [5] and wideband radar cross section (RCS) reduction [6], [7]. Therefore, developing effective and efficient FSS techniques or structures is conducive to meeting these stringent requirements.

Several kinds of FSS methods or structures have been reported, including single-layer FSSs, multilayer FSSs, and 3-D FSSs. Traditional single-layer FSSs are composed of two-dimensional periodic arrays based on resonant structures, such as dipoles, slots, loops, patches, and their derivatives [1]. Even though some combined structures [8], miniaturization methods [9], [11], and multiple-mode resonator (MMR) techniques [10] are utilized to improve the performance of single-layer FSSs, poor skirts and a narrow working bandwidth is commonly attributed due to their limited resonant modes. To obtain a high-order filtering response for sharp skirts, different single-layer FSSs are cascaded to form multilayer FSSs. In [12], a two-layer FSS is designed and validated for bandwidth improvement compared with a single-layer FSS. Some three-layer FSSs composed of two capacitive patches and one inductive wire grid are stacked to achieve two-order [13], fast roll-off [14], three-order [15], and dual-band [16] filtering responses. These multiplayer FSSs indeed exhibit a higher order filtering response compared with single-layer FSSs. However, they have only a single function and are unsuitable for practical applications. To obtain advanced filtering performance, 3-D FSSs have been investigated by employing transmission lines or waveguide structures [17], such as coaxial waveguides and parallel-plate waveguides [18], slot lines and microstrip lines [19], [20], [21], [22], [23], [24], parallel-strip lines [25], and substrate integrated waveguides

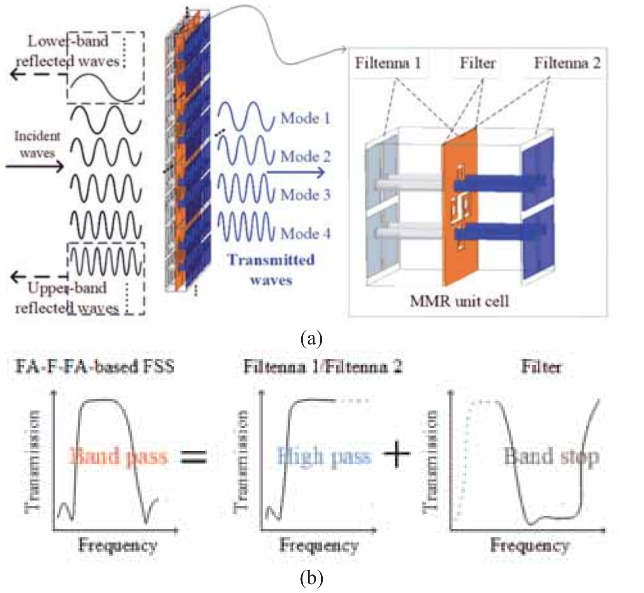

Fig. 1. (a) Schematic of the proposed FSS using MMRs and the FA-F-FA-based MMR unit cell. (b) Working principle of the bandpass filtering response of the FA-F-FA-based FSS.

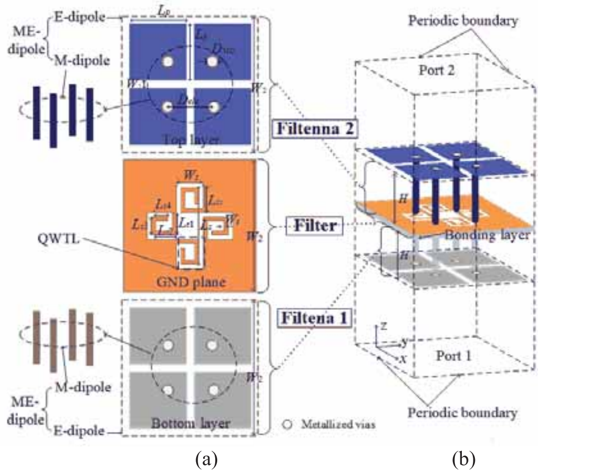

Fig. 2. Geometry of (a) Filtennas 1 and 2 and the filter-embedded GND plane with QWTLs. (b) Three-dimensional view of the MMR unit cell of the proposed FA-F-FA-based FSS. [Physical dimensions (units: mm): $L_{\rm p} = 2.1$, $L_{\rm s} = 3$, $L_{\rm s2} = 1.025$, $L_{\rm r1} = 0.8$, $L_{\rm r2} = 0.875$, $L_{\rm r3} = 0.65$, $L_{\rm r4} = 0.575$, $W_1 = 0.3$, $W_2 = 4.7$, $W_{\rm s} = 0.95$, $W_{\rm r} = 0.15$, $D_{via} = 0.4$, $D_{ele} = 1.7$, and $H = 1.524$].

(SIWs) [26], [27], [28], [29]. Although these methods and structures are attractive filtering performances, they suffer from either complex structures or poor out-of-band performance. Therefore, it is still necessary to investigate on FSSs with a simple, low-profile, and wide upper stopband characteristic.

Alternatively, an FSS technique has been gradually concerned from an antenna-filter-antenna (AFA) point of view. It comprises receiving antennas, filtering structures, and transmitting antennas [30], [31], [32]. The filtering responses of the AFA-based FSSs mainly depend on the filtering structures. By modifying the filtering coplanar-waveguide resonators, three different bandpass FSSs can be accomplished [30]. A miniaturized bandpass FSS [31] and a five-layer FSS [32] are designed based on the AFA concept. Since the filtering response of AFA-based FSS is achieved by designing the filtering structures only, the AFA-based FSSs usually suffer from a poor filtering response due to the limited design freedom. In [33], radiation nulls of the patch antenna and a filtering slot on the GND plane are used to accomplish an elliptical filtering response. However, this method is only suitable for single-polarized applications. Moreover, both the passband bandwidth and the upper stopband bandwidth are relatively narrow. To achieve a wide passband bandwidth and a high filtering selectivity, filtenna-to-filtenna (FA-FA)-based FSS [34] is recently proposed using a back-to-back magnetoelectric (ME)-dipole antenna array. The bandwidth of out-of-band rejection is yet narrow, especially the upper stopband improvement required.

This article investigates on a novel filtenna-filter-filtenna (FA-F-FA)-based FSS with simultaneously a wide bandpass and two wide stopbands using MMRs. The simplified design principle is shown in Fig. 1. The MMR unit cell of FSS consists of two identical filtennas connected by a filter-embedded GND plane. In this way, an FA-F-FA-based FSS is formed by arraying the unit cell. The filtering response of the FA-F-FA-based FSS takes advantage of the two filtennas and the filter-embedded GND plane, and more design freedom for the filtering response can be obtained, resulting in a high-order filtering response and a wide out-of-band rejection. In addition, the design can be integrated into a printed circuit board (PCB) laminate without manual assembly, which means that additional pins and screws for installation are not required.

This article is organized as follows. The FSS design process, the geometry of filtennas, filter, and the unit cell of the FSS, and the S-parameters of the FSS are given in Section II. The modes of filtenna, filter, and the proposed FSS are discussed in Section III. The out-of-band rejection in the lower and upper bands and the cross polarizations are analyzed in Section IV. Section V presents the FSS design guideline, the measurement results of the FSS, and the figure-of-merit comparison. A conclusion is given in Section VI.

II. FSS Design

Fig. 1(a) shows the structures of the proposed FSS and the FA-F-FA-based MMR unit cell, where the desired incident waves with specific frequencies are selected to pass through by the MMRs of the FSS, while the undesired waves are reflected. The bandpass response of the FSS depends on the two high-pass filtennas and a stopband filter, as shown in Fig. 1(b). The two back-to-back filtennas can be treated as a single MMR, and this property will be shown in Section III. Then, a filter-embedded GND plane with four quarter-wavelength transmission lines (QWTLs) is proposed to improve the out-of-band performance. In this section, the MMR unit cell of the FSS, including Filtennas 1 and 2 and the filter, will be introduced in detail. Then, the FA-F-FA-based FSS will be eventually arrayed using a periodic boundary condition, and its final filtering response under a normal-incidence TE wave will be illustrated.

A. Filtennas 1 and 2

The geometries of Filtennas 1 and 2 elements are shown in the upper and lower parts of Fig. 2(a), respectively. They are ME-dipole antennas with identical structures, exhibiting an intrinsic high-pass filtering response [34] and wide working bandwidth by taking advantage of the combination of magnetic (M)-dipole mode and electric (E)-dipole mode [36], [37], [38], [39], [40]. Different from the ME-dipole antenna styles in [35], [36], [37], [38], [39], and [40], the proposed filtenna element is integrated into a PCB laminate to simplify the fabrication complexity. The ME-dipole consists of an E-dipole and an M-dipole. The E-dipole antenna is formed by etching four identical square patches on top of the 1.524-mm RO4350 substrate with a relative permittivity of 3.66, where four identical vertical metallic vias are utilized to form the M-dipole antenna. Dual polarization is achievable by the symmetric structure of the ME-dipole antenna along the x- and y-axes.

B. Filter

The structure of the filter is shown in the center part of Fig. 2(a), which is composed of a cross-slotted GND plane and four rotationally symmetric QWTLs, where the wavelength is at the frequency of transmission zero (TZ) in the upper band of the FSS. The total length of each QWTL is the sum of L_{r1}, L_{r2}, L_{r3}, and L_{r4}. On the one hand, when the QWTLs resonant, no electromagnetic waves can pass through the slots, resulting in a TZ in the upper band of the FSS. On the other hand, the slots act as a bandpass filter, passing the resonant frequency of the slots and rejecting the lower and upper frequencies [1]. Therefore, the length of the slots controls the passband response of the FSS. At the same time, as the common GND plane of Filtennas 1 and 2, the filter plays an important role in impedance matching for Filtennas 1 and 2.

C. FA-F-FA-Based FSS

The MMR unit cell of the proposed FA-F-FA-based FSS is formed by combining Filtennas 1 and 2, and the filter-embedded GND plane is shown in Fig. 2(b), where Filtennas 1 and 2 are connected back to back by the filter. Filtenna 1 is built on a 1.524-mm RO4350 substrate, while Filtenna 2 and the filter are built on another identical RO4350 substrate. A 0.1-mm Rogers RO4450F with a reflective dielectric of 3.55 is used to bond the two substrates. The detailed dimensions of the MMR unit cell of the FSS are listed in Fig. 2.

With the help of full-wave electromagnetic solver HFSS, the periodic boundary condition is employed to analyze the proposed FSS. The simulated S-parameters of the FSS under normal-incidence TE waves are shown in Fig. 3. Since the structure of the FSS is symmetrical along the x-axis and y-axis, the S-parameters under normal-incidence TE and TM waves are the same. Therefore, only S-parameters under a normal-incidence TE wave are here for brevity. As shown in Fig. 3, $|S_{11}|$ and $|S_{22}|$ are the same due to the identical structure of Filtennas 1 and 2. Therefore, only $|S_{11}|$ will be given in the following sections for simplification. Four transmission

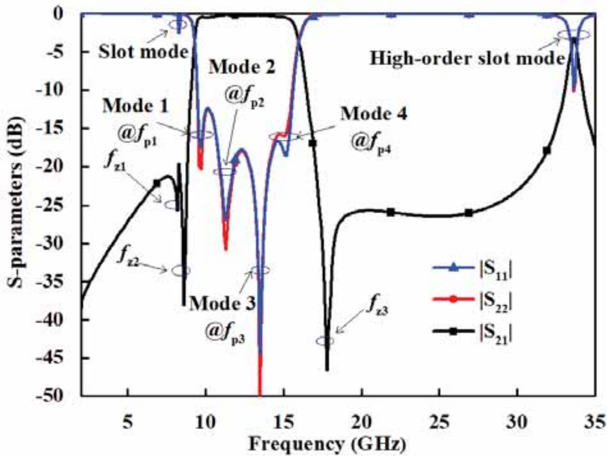

Fig. 3. Simulated S-parameters of the FA-F-FA-based FSS under normal-incidence TE waves.

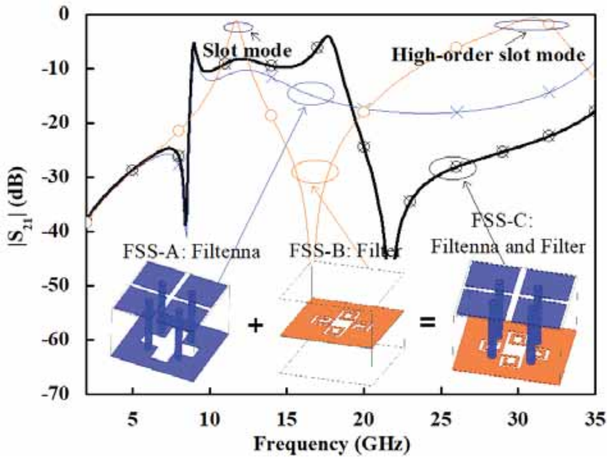

Fig. 4. Transmission coefficients of FSS-A, FSS-B, and FSS-C.

modes (i.e., Modes 1–4) in the passband are obtained, leading to a wide passband. The slot mode at the lower band edge is suppressed at a very low level by being properly located at the TZ, and three TZs at f_{z1}, f_{z2}, and f_{z3} are obtained, exhibiting a wide out-of-band rejection.

III. Multiple Modes of FSS

In this section, the S-parameters for FSS-A, FSS-B, and FSS-C are first given to illustrate the multiple modes of the FA-F-FA-based FSS. Then, the current and electric field distributions of the FA-F-FA-based FSS are further analyzed to demonstrate the multiple modes of the proposed FSS.

A. Modes of the Filtennas and the Filter

MMRs have been widely used in ultrawideband (UWB) bandpass filters due to the multiple adjacent resonance modes [41], [42]. Similarly, MMRs are used to obtain a wide passband of the proposed FA-F-FA-based FSS in this work. To illustrate the multiple modes of the proposed FSS, three kinds of FSSs are designed and analyzed in Fig. 4. The unit cell of FSS-A consists of the proposed filtenna element and

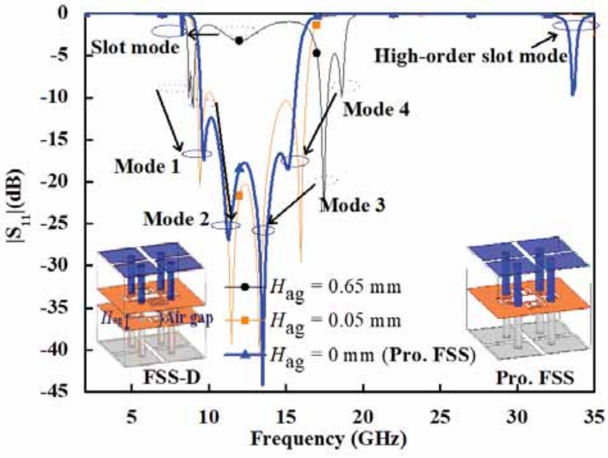

Fig. 5. Resonance modes of the FSS-D with different air gaps compared with the modes of the proposed FSS.

a cross-slotted GND plane without QWTLs, while the unit cell of FSS-B comprises the proposed filter element and two identical 1.524-mm RO4350 substrates. Similarly, the unit cell of FSS-C is made up of the proposed filtenna element and the proposed filter element. The simulated $|S_{21}|$ of the three FSSs is also plotted in Fig. 4. For FSS-A, two transmission modes can be observed. For the FSS-B, fundamental and high-order slot modes are found. Taking full advantage of the two modes of FSS-A and the fundamental slot mode of FSS-B, three transmission modes can be obtained for FSS-C.

To further investigate the multiple modes of the proposed FSS, FSS-D is designed and compared with the proposed FSS in Fig. 5. The unit cell of FSS-D is composed of two back-to-back FSS-Cs and separated by an air gap. The simulated $|S_{11}|$ of FSS-D with different separations (H_{ag}) is depicted here. When $H_{ag} = 0.65$ mm, Modes 1–4, a slot mode among them occurs. The slot mode is formed by the slots on the GND plane, while the four modes are caused by Filtennas 1 and 2. When H_{ag} decreases from 0.65 to 0.05 mm, Modes 1–4 move close to the center frequency and have better impedance matching, while the slot mode moves to the lower frequency due to strong coupling. Finally, Modes 1–4 of the proposed FA-F-FA-based FSS can be obtained in the passband when connecting the two FSS-Cs (i.e., $H_{ag} = 0$ mm).

B. Modes of the FA-F-FA-Based FSS

To demonstrate the multiple modes of the proposed FA-F-FA-based FSS, the current distributions on the top and bottom layers of the proposed FSS at the frequencies of f_{p1}, f_{p2}, f_{p3}, and f_{p4} are given in Fig. 6. The bottom layer is excited under a normal-incidence TE wave. It should be pointed out that only the detailed current distributions at $t = 0$ are given here for brevity. In Fig. 6, the E-mode, parallel to the TE wave, represents that the E-dipole is strongly excited, as depicted with a red solid arrow, while the M-mode, perpendicular to the TE wave, means that the M-dipole is strongly excited, as indicated by a black dashed arrow. The modes of current distributions of the FSS at $t = 0$, T/8, T/4, and 3T/8 are listed in Table I, where T is the period of the current distributions

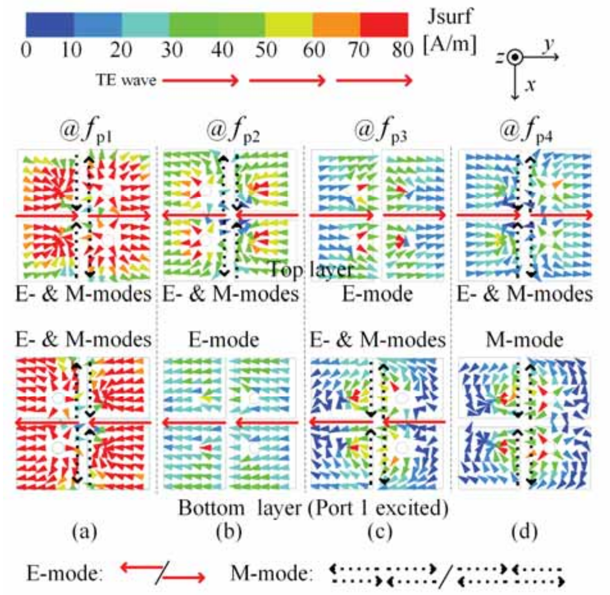

Fig. 6. Current distributions of the four modes on the bottom and top layers of the proposed MMR FSS with $t = 0$. (a) Mode 1 at f_{p1}. (b) Mode 2 at f_{p2}. (c) Mode 3 at f_{p3}. (d) Mode 4 at f_{p4}.

TABLE I

MODES ON THE BOTTOM AND TOP LAYERS OF THE PROPOSED FSS WITH DIFFERENT FREQUENCIES AND TIMES

	(Bottom-layer modes) - (Top-layer modes)			
$t =$	Mode 1 @ f_{p1}	Mode 2 @ f_{p2}	Mode 3 @ f_{p3}	Mode 4 @ f_{p4}
0	(E&M)-(E&M)	(E)-(E&M)	(E&M)-(E)	(M)-(E&M)
T/8	(E&M)-(E&M)	(E&M)-(E)	(E)-(E&M)	(E)-(E)
T/4	(E&M)-(E&M)	(E&M)-(E)	(E)-(E&M)	(E)-(E)
3T/8	(E&M)-(E&M)	(M)-(E&M)	(E&M)-(E)	(E&M)-(M)

T: Period of the current distributions.
E: E-mode; M: M-mode.

caused by the proposed FSS. Since the modes have a period of T/2, the modes at times from 0 to 3T/8 listed in Table I can adequately represent the modes of the FSS in the whole period. It can be observed that four different combination modes, comprised of E-mode, M-mode, and the hybrid E- and M-modes on both the top and bottom layers of the FSS, are achieved, resulting in four modes at f_{p1}, f_{p2}, f_{p3}, and f_{p4}.

To further illustrate the four modes of the proposed FA-F-FA-based FSS, the electric field distributions of the E-plane of the proposed FSS under the normal-incidence TE wave are introduced, as shown in Fig. 7. Port 1 is excited. The blue solid arrows represent the inner electric field of a unit cell, while the black dashed arrows show the mutual-coupling electric field between adjacent unit cells. It can be observed that the electric fields of each unit cell mainly include E1±, E2±, E3±, and E4±, where the "+" and "−" represent the +y and −y directions of the electric field, respectively. E1± and E3± are the inner electric field of each unit cell, while

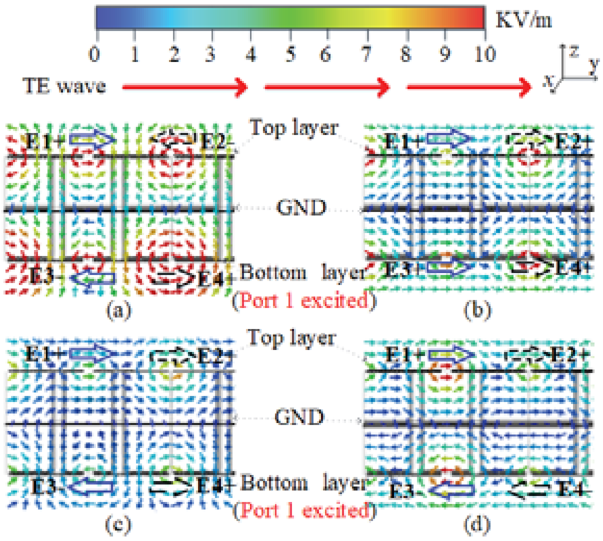

Fig. 7. Electric field distributions of the E-plane of the proposed MMR FSS: (a) Mode 1 at f_{p1}, (b) Mode 2 at f_{p2}, (c) Mode 3 at f_{p3}, and (d) Mode 4 at f_{p4}. Blue solid arrow: inner electric field of a unit cell; Black dashed arrow: mutual-coupling electric field between the adjacent unit cells.

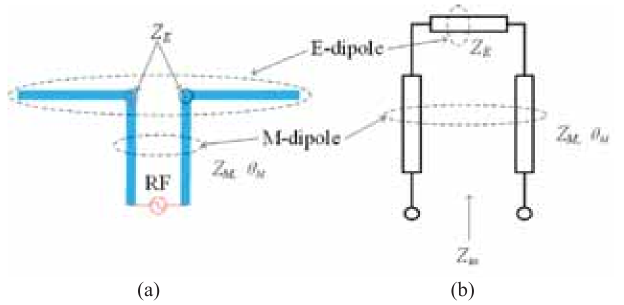

Fig. 8. (a) ME-dipole antenna model. (b) Its simplified equivalent circuit model.

E2± and E4± are the mutual-coupling electric field between the adjacent unit cells. Four modes based on electric fields are realized, i.e., Mode 1 (E1+, E2−, E3−, and E4+) in Fig. 7(a), Mode 2 (E1+, E2+, E3+, and E4+) in Fig. 7(b), Mode 3 (E1+, E2+, E3−, and E4+) in Fig. 7(c), and Mode 4 (E1+, E2+, E3−, and E4−) in Fig. 7(d).

In summary, the four modes of the proposed FSS at f_{p1}, f_{p2}, f_{p3}, and f_{p4} can be analyzed with different current and electric field combinations. Therefore, the wide passband for the proposed FSS is achieved based on the four modes.

IV. Out-of-Band Rejection

This section demonstrates the operation mechanism of out-of-band rejection in the lower and upper bands. First, the equivalent circuit of ME-dipole antennas is adapted to illustrate the lower band TZs of the proposed FSS, and the length of the slots on the GND plane is adjusted to improve the lower band rejection by suppressing the fundamental slot mode. Finally, upper band TZs, upper band rejection, and cross polarizations are investigated after embedding the rotationally symmetric QWTLs into the GND plane.

A. Lower Band Rejection

The lower band rejection is analyzed by an equivalent circuit model of Filtennas 1 and 2, as shown in Fig. 8(a). Due to the identical structures of Filtennas 1 and 2, only one of the models is given here. Since the two filtennas are traditional ME-dipole antennas, consisting of an E-dipole and an M-dipole, they can be equivalent to a series circuit composed of an E-dipole antenna and an M-dipole antenna. Therefore, the equivalent circuit consists of a load Z_E and a transmission line with a phase of θ_M and a characteristic impedance of Z_M, as shown in Fig. 8(b). Z_E represents the input impedance of the E-dipole, while Z_M and θ_M represent the characteristic impedance and the phase of the M-dipole, respectively. Then, the input impedance of filtennas can be calculated by the following impedance transformation equation [43]:

$$Z_{in} = Z_M \frac{Z_E + jZ_M \tan\theta_M}{Z_M + jZ_E \tan\theta_M}. \tag{1}$$

When $Z_{in} = 0$ or $Z_{in} = \infty$, two TZs of the FSS will be obtained due to the two back-to-back filtennas [34]. Therefore, (1) can be simplified as

$$Z_M \tan\theta_M = jZ_E \quad (Z_{in} = 0) \tag{2}$$

or

$$Z_M \cot\theta_M = -jZ_E \quad (Z_{in} = \infty). \tag{3}$$

Fixing the value of Z_E, Z_M and θ_M of M-dipole can be used to adjust the TZs of the FSS. Here, θ_M and Z_M can be calculated as follows:

$$\theta_M = 2\pi H/\lambda_g \tag{4}$$

$$Z_M = \frac{60}{\sqrt{\epsilon_r}} arcosh\left(\frac{S_{ele}}{D_{via}}\right). \tag{5}$$

For (4), H and λ_g represent the height of the M-dipole antenna and the wavelength of the electromagnetic wave in the substrate, respectively. For (5), Z_M can be equivalent to a half characteristic impedance of a parallel transmission line [43]. S_{ele} and D_{via}, respectively, represent the center spacing of two adjacent vias elements and the diameter of the vias. Therefore, the height (H) of the M-dipole antenna and the diameter (D_{via}) of the vias can be used to control the two TZs of the FSS.

To analyze the TZs in the lower rejection band, simulated S-parameters of the FSS with different H and D_{via} are shown in Fig. 9(a) and (b), respectively. When H elevates from 1.324 to 1.524 mm, the two TZs move to lower frequencies; when the diameter of the vias rises from 0.2 to 0.4 mm, the two TZs shift to higher frequencies.

To further investigate the lower band rejection, simulated S-parameters of the FSS with different lengths (L_s) of the slots are shown in Fig. 10. As mentioned before, the slots in the GND plane keep a bandpass response at their resonance frequencies. Similarly, the length of the slots can be adjusted to control the lower band rejection by suppressing the slot mode. In Fig. 10, when L_S decreases from 3.8 to 3.0 mm, the slot mode is gradually suppressed in the lower rejection band. This

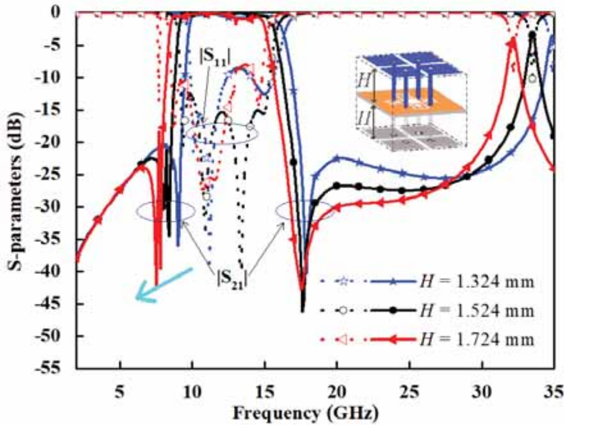

(a)

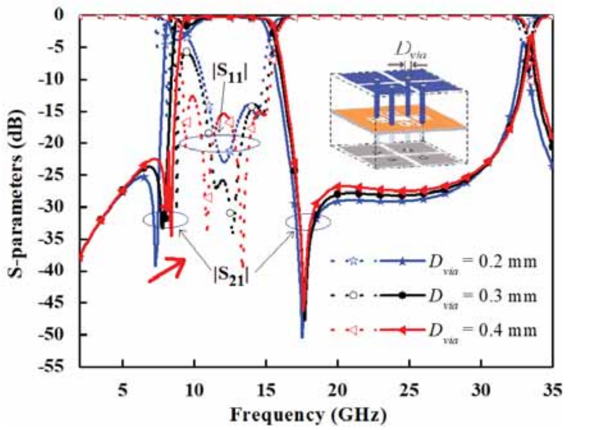

(b)

Fig. 9. Simulated S-parameters of the proposed FSS with. (a) Height (H) of filtennas. (b) Diameter (D_{via}) of the shorted metallized vias.

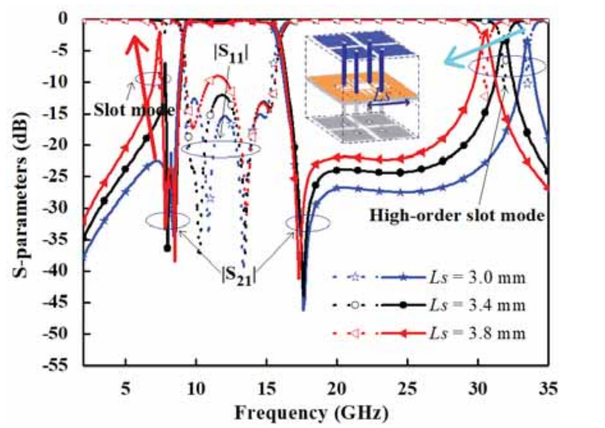

Fig. 10. Simulated S-parameters of the proposed FSS with different lengths (L_s) of the slots on the GND plane.

is because the slot mode in the lower frequency moves to the TZs in the lower band edge. To obtain a wider lower rejection band, the slot mode in the rejection band should be prohibited. Therefore, the length of the slots should be elaborated.

In short, the TZs in the lower rejection band can be controlled by adjusting the height of the M-dipole antenna and the diameter of the vias. Also, the lower band rejection can be improved by elaborating the length of the slots in the GND plane.

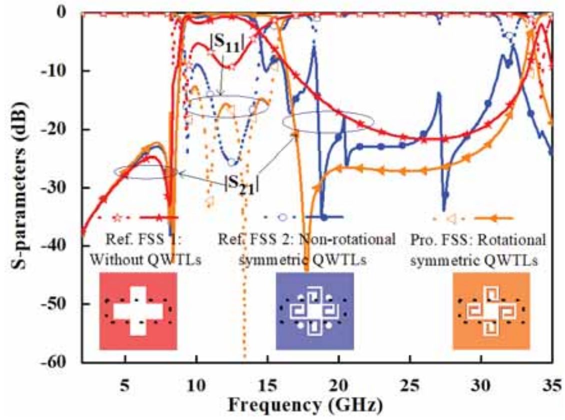

Fig. 11. Structure and the simulated S-parameters of Ref. FSS 1, Ref. FSS 2, and the proposed FSS. (Filtennas 1 and 2 are not given for brevity.)

B. Upper Band Rejection

To analyze the upper band rejection, Ref. FSS 1 and Ref. FSS 2 are introduced for comparison with the proposed FSS, as shown in Fig. 11. The three FSSs consist of Filtennas 1 and 2, and GND plane, where Filtennas 1 and 2 are not given for brevity. The only difference between Ref. FSS 1 and the proposed FSS is that Ref. FSS 1 is without the QWTLs on the GND plane, and other parameters remain the same for better comparison. The simulated S-parameters of the two FSSs are shown in Fig. 11. It can be observed that a sharp TZ and wider upper rejection band can be obtained for the proposed FSS, while there are no sharp TZs and wide upper rejection bands for Ref. FSS 1. What is more, only two TPs can be obtained for Ref. FSS 1. This is because the GND plane without QWTLs has a limited matching for Filtennas 1 and 2 of Ref. FSS 1. In a word, the QWTLs on the GND plane act as a stopband filter in the upper rejection band and a matching network for Filtennas 1 and 2.

For Ref. FSS 2, the four QWTLs in the cross slots are nonrotationally symmetric, while for the proposed FSS, the QWTLs are rotationally symmetric. Similarly, other structures, dimensions, and materials remain the same for the two FSSs. However, some undesired harmonic waves occur in the upper band edge and upper rejection band for Ref. FSS 2, resulting in an inadequate upper band filtering response, as shown in Fig. 11. The undesired filtering response is caused by the cross polarizations for Ref. FSS 2, and it will be illustrated in the following.

The TZ at f_{z3} in the upper rejection band can be obtained when the QWTLs resonate. f_{z3} can be approximately calculated by [43]

$$f_{z3} = \frac{c}{4L_r\sqrt{\varepsilon_{eff}}} \tag{6}$$

where c is the velocity of the electromagnetic wave in the air, ε_{eff} represents the effective dielectric constant of the substrate, and L_r is the total length of each QWTL, in which L_r is the

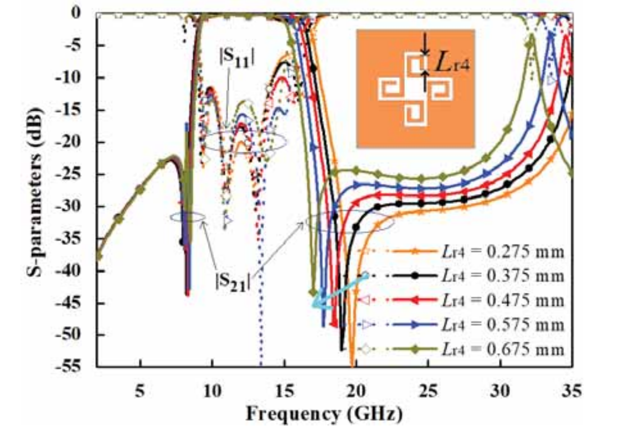

Fig. 12. S-parameters of the proposed FSS with different lengths L_{r4} of QWTLs. (Filtennas 1 and 2 are not given for brevity.)

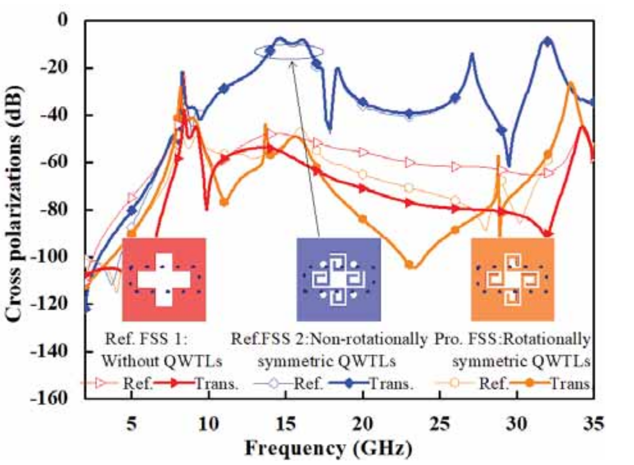

Fig. 13. Cross polarizations of Ref. FSS 1, Ref. FSS 2, and the proposed FSS. (Filtennas 1 and 2 are not given for brevity.)

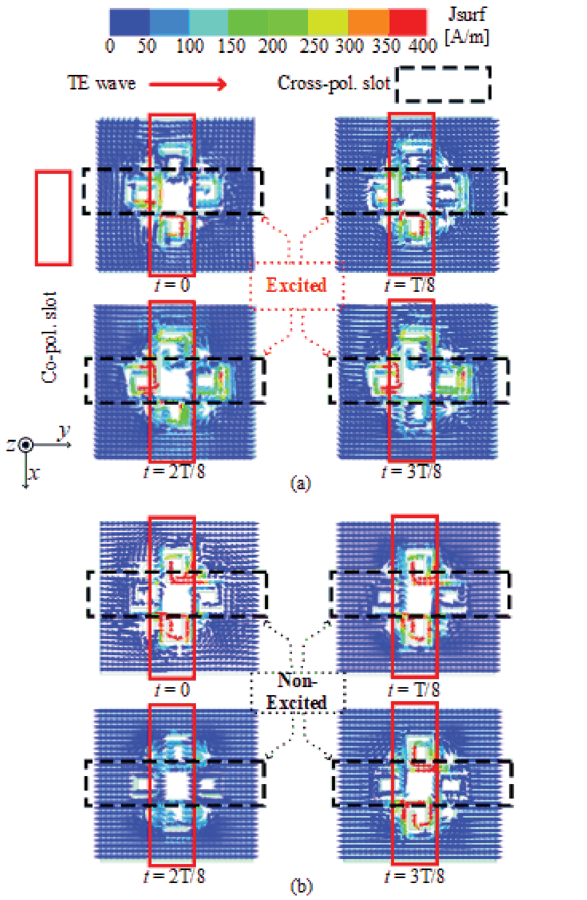

Fig. 14. Current distributions on GND planes of (a) Ref. FSS 2. (b) Proposed FSS under normal-incident TE wave with different times at 15.3 GHz (T represents the period of current distributions).

sum of L_{r1}, L_{r2}, L_{r3}, and L_{r4}. As shown in Fig. 12, the partial length L_{r4} of QWTLs is adjusted to control the TZ in the upper rejection band. When L_{r4} rises from 0.275 to 0.675 mm, f_{z3} decreases from 19.7 to 17.0 GHz, which confirms (6).

C. Cross Polarizations

The cross polarizations for the three FSSs are studied in Fig. 13. For Ref. FSS 2, it can be observed that there are the largest cross-polarization reflection and transmission around the upper band edge, while both the proposed FSS and Ref. FSS 1 have a low cross-polarization level for both reflection and transmission, which indicates that the proposed rotationally symmetric QWTLs are with distinguished performance in cross polarizations.

To further analyze and compare the cross-polarization behaviors of Ref. FSS 2 and the proposed FSS, the current distributions on the GND plane of the two FSSs are compared at different times during the period of the current distributions, as shown in Fig. 14. The two FSSs are excited by a normal-incidence TE wave at 15.3 GHz, which is in the upper band edge. The red solid rectangle and the black dotted rectangle represent the co-polarization slot and cross-polarization slot, respectively.

For Ref. FSS 2, the QWTLs in both the co-polarization slot and cross-polarization slot have been excited with the times from 0 to 3T/8, resulting in a large cross polarization of Ref. FSS 2. For the proposed FSS, the QWTLs only in the co-polarization slot are excited, and the current on the QWTLs is with a weak magnitude and opposite phase, leading to a small cross polarization for the proposed FSS. In other words, the rotationally symmetric QWTLs can suppress the cross polarizations efficiently. Therefore, the rotationally symmetric QWTLs in the GND plane play a key role in improving the cross-polarization performance of the proposed FSS, compared with Ref. FSS 2.

V. Implementation and Measurement

A. Design Procedure

The design procedure for the proposed FA-F-FA-based FSS can be summarized in four steps as follows.

1) *Filtenna Element:* An ME-dipole antenna is selected as a high-pass filter. The total lengths of the E-dipole antenna and M-dipole antenna are about a quarter waveguide wavelength at the center frequency of the passband.

TABLE II
FIGURE-OF-MERIT COMPARISON OF THE FSSS UNDER NORMAL-INCIDENCE WAVES

Ref.	FSS structures	f_0 (GHz)	Order	Lower-band FBW_{20dB}	In-band FBW_{3dB}	Upper-band FBW_{20dB}	Single/dual polarization	Angular stability	Loss tangent	Insertion loss (dB)
[13]	Multilayer FSS	10	2	10%	25%	22%	Dual	30°	0.0027	0.3
[14]	Multilayer FSS	3.8	2	9%	10%	8%	Dual	40°	0.019	1.05
[28]	SIW FSS	30	2	8.8%	4.5%	1%	Dual	40°	0.0009	2.5
[29]	SIW FSS	10.14	3	3.7%	1.7%	1.8%	Dual	40°	0.0027	~2
[31]	AFA-based FSS	5.05	2	1.1%	9.4%	0	Dual	30°	0.0009	0.9
[33]	AFA-based FSS	9.71	2	4.5%	9.3%	0.5%	Single	20°	0.0027	~0.5
[34]	FA-FA-based FSS	11.64	3	8.7%	38.5%	13.8%	Dual	40°	0.004	0.19
Our work	**FA-F-FA-based FSS**	**12.27**	**4**	**53.5%**	**50.2%**	**119.2%**	**Dual**	**50°**	**0.004**	**0.29**

$FBW_{3dB} = [Bandwidth\ of\ |S_{21}| \geq -3dB]/f_0 \times 100\%$ $\quad FBW_{20dB} = [Bandwidth\ of\ |S_{21}| \leq -20dB]/f_0 \times 100\%$

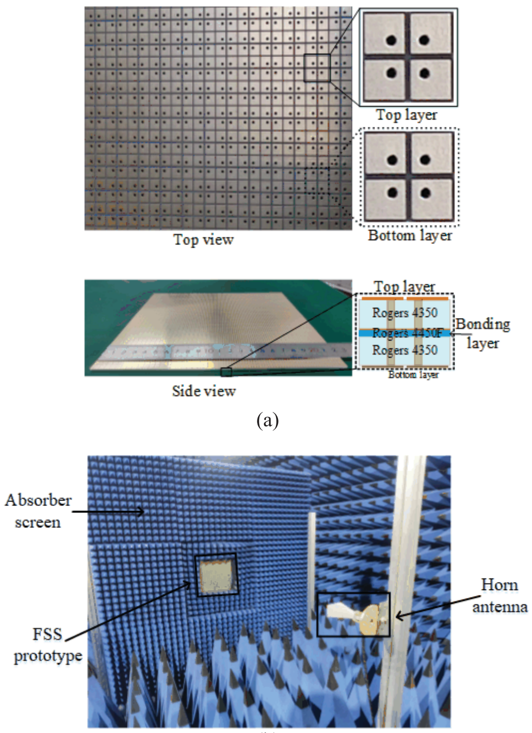

Fig. 15. (a) Photograph of the prototype of proposed FA-F-FA-based FSS. (b) Measurement setup in the anechoic chamber.

2) *Filtering and Matching GND Plane:* The four QWTLs are rotationally symmetric, and the total length of each QWTL is close to a quarter waveguide wavelength at the frequency of transmission zero in the upper band of the FSS.
3) *Symmetric FA-F-FA Unit Cell:* Symmetric cross slots are used to make Filtennas 1 and 2, and the GND plane symmetric along the x-axis and y-axis. The two filtennas are connected by the through-holed GND plane back to back.
4) *FSS Design:* The periodic boundary condition is employed to analyze the proposed FSS.

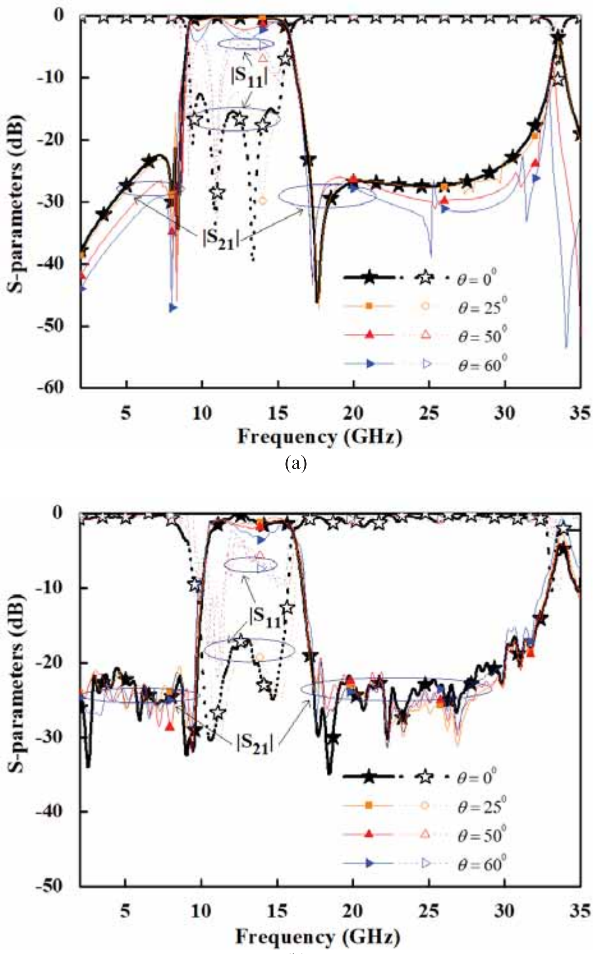

Fig. 16. S-parameters of the proposed FSS under TE waves with different incidence angles of 0°, 25°, 50°, and 60°. (a) Simulated. (b) Measured.

B. Measured Results

Fig. 15(a) shows the prototype of the proposed FSS. The overall size of the prototype is 220.9 × 220.9 × 3.148 mm [9.03 λ_0 × 9.03 λ_0 × 0.13 λ_0 (λ_0 is the free-space wavelength at the center frequency of 12.27 GHz)], consisting of 47 × 47 unit cells. The measurements are carried out in an anechoic chamber to avoid interference signals, as shown in Fig. 15(b).

Since the S-parameters under TE and TM waves are almost the same due to the symmetric structure of the proposed FSS, therefore, only S-parameters under the TE waves are given here for brevity. The simulated and measured S-parameters of the FSS under TE waves with different incidence angles of 0°, 25°, 50°, and 60° are compared in Fig. 16. It can be observed that the S-parameters keep good angular stability from 2 to 35 GHz under 50° incident angle. Also, the measured results and the simulated ones are in good agreement.

C. Comparison

Some classic and recently published FSSs are listed in Table II for the figure-of-merit comparison. Compared with multilayer FSSs, SIW FSSs, AFA-based FSSs, and FA-FA-based FSS, the proposed FA-F-FA-based FSS is with higher order, wider rejection band, wider passband, and better angular stability. What is more, compared with [13], [28], [29], [31], and [33], the insertion loss of our work is the lowest even though the substrate of our work has the highest loss tangent. With all these merits, the proposed FA-F-FA-based FSS is promising as a new FSS technique with high-order filtering response, wide passband, and wide out-of-band rejection.

VI. Conclusion

In this article, a new FA-F-FA-based FSS method has been proposed using MMRs. The method is realized by using an MMR array composed of back-to-back ME-dipole antennas and a filter-embedded GND plane without increasing the unit cell size. The lower rejection band of the proposed FSS depends on the inherent lower transmission null of ME-dipole antennas and the length of slots. The QWTLs on the GND plane control the upper rejection band. Moreover, the introduction of QWTLs does not deteriorate the cross-polarization level of the FSS. The wide passband benefits from four modes of the FSS. The wide-passband, wide-rejection-band, and high-order filtering performances are obtained using the FA-F-FA-based structure. In addition, it has the advantages of dual-polarization application and assembly free based on the PCB process. Therefore, the proposed FA-F-FA-based FSS using MMRs is a promising candidate for the new FSS technology.

References

[1] B. A. Munk, *Frequency Selective Surfaces: Theory and Design*. New York, NY, USA: Wiley, 2000.

[2] Z. Xing, F. Yang, P. Yang, and J. Yang, "A low-RCS and wideband circularly polarized array antenna co-designed with a high-performance AMC-FSS radome," *IEEE Antennas Wireless Propag. Lett.*, vol. 21, no. 8, pp. 1659–1663, Aug. 2022.

[3] X. Li, Z. Zhou, Q. Wang, and J. Zhang, "A polarization conversion radome for high-power microwave applications," *IEEE Antennas Wireless Propag. Lett.*, vol. 18, no. 6, pp. 1096–1099, Jun. 2019.

[4] M. Li and N. Behdad, "Wideband true-time-delay microwave lenses based on metallo-dielectric and all-dielectric lowpass frequency selective surfaces," *IEEE Trans. Antennas Propag.*, vol. 61, no. 8, pp. 4109–4119, Aug. 2013.

[5] J. Hu, H. Wong, and L. Ge, "A circularly-polarized multi-beam magneto-electric dipole transmitarray with linearly-polarized feeds-based for millimeter-wave applications," *IEEE Trans. Antennas Propag.*, vol. 70, no. 7, pp. 6012–6017, Jul. 2022.

[6] Y. Pang et al., "Wideband RCS reduction metasurface with a transmission window," *IEEE Trans. Antennas Propag.*, vol. 68, no. 10, pp. 7079–7087, Oct. 2020.

[7] E. F. Knott, J. F. Schaeffer, and M. T. Tulley, *Radar Cross Section*. Raleigh, NC, USA: SciTech Pub., 2004.

[8] T. Hong, W. Xing, Q. Zhao, Y. Gu, and S. Gong, "Single-layer frequency selective surface with angular stability property," *IEEE Antennas Wireless Propag. Lett.*, vol. 17, no. 4, pp. 547–550, Apr. 2018.

[9] S. S. Sampath and R. Sivasamy, "A single-layer UWB frequency-selective surface with band-stop response," *IEEE Trans. Electromagn. Compat.*, vol. 62, no. 1, pp. 276–279, Feb. 2020.

[10] N. Jawad and L. Markley, "A single-layer frequency selective surface with dual wideband band-stop response," *IEEE Antennas Wireless Propag. Lett.*, vol. 19, no. 6, pp. 916–920, Jun. 2020.

[11] M. Qu, Y. Feng, J. Su, and S. Mohsin Ali Shah, "Design of a single-layer frequency selective surface for 5G shielding," *IEEE Microw. Wireless Compon. Lett.*, vol. 31, no. 3, pp. 249–252, Mar. 2021.

[12] A. L. P. de Siqueira Campos, R. H. C. Maniçoba, and A. G. d'Assunção, "Investigation of enhancement band using double screen frequency selective surfaces with koch fractal geometry at millimeter wave range," *J. Infr., Millim., THz Waves*, vol. 31, no. 12, pp. 1503–1511, Dec. 2010.

[13] M. Al-Joumayly and N. Behdad, "A new technique for design of low-profile, second-order, bandpass frequency selective surfaces," *IEEE Trans. Antennas Propag.*, vol. 57, no. 2, pp. 452–459, Feb. 2009.

[14] M. Hussein, J. Zhou, Y. Huang, and B. Al-Juboori, "A low-profile miniaturized second-order bandpass frequency selective surface," *IEEE Antennas Wireless Propag. Lett.*, vol. 16, pp. 2791–2794, 2017.

[15] M. Li and N. Behdad, "A third-order bandpass frequency selective surface with a tunable transmission null," *IEEE Trans. Antennas Propag.*, vol. 60, no. 4, pp. 2109–2113, Apr. 2012.

[16] M. B. Yan et al., "A miniaturized dual-band FSS with second-order response and large band separation," *IEEE Antennas Wireless Propag. Lett.*, vol. 14, pp. 1602–1605, 2015.

[17] A. K. Rashid, B. Li, and Z. Shen, "An overview of three-dimensional frequency-selective surfaces," *IEEE Antennas Propag. Mag.*, vol. 56, no. 3, pp. 43–67, Jun. 2014.

[18] J. Zhu, W. Tang, C. Wang, C. Huang, and Y. Shi, "Dual-polarized bandpass frequency-selective surface with quasi-elliptic response based on square coaxial waveguide," *IEEE Trans. Antennas Propag.*, vol. 66, no. 3, pp. 1331–1339, Mar. 2018.

[19] W. Zhang, B. Li, L. Zhu, Y.-P. Lyu, and C.-H. Cheng, "Stacked slotline structure-based unit cell and its application for synthesis of 3-D bandpass frequency-selective surfaces," *IEEE Trans. Antennas Propag.*, vol. 68, no. 12, pp. 7958–7968, Dec. 2020.

[20] W. Zhang, B. Li, L. Zhu, X. Zhao, Y.-P. Lyu, and C.-H. Cheng, "Synthesis design of bandpass frequency selective surface with multiple transmission zeros using slotline structures," *IEEE Trans. Antennas Propag.*, vol. 70, no. 10, pp. 9449–9459, Oct. 2022.

[21] B. Li et al., "Bandpass frequency selective structure with improved out-of-band rejection using stacked single-layer slotlines," *IEEE Trans. Antennas Propag.*, vol. 66, no. 11, pp. 6003–6014, Nov. 2018.

[22] B. Li, L. Zhu, Y. Tang, Y. Chang, Y. Han, and Y. Lyu, "Wideband frequency selective structures based on stacked microstrip/slot lines," in *Proc. Int. Conf. Microw. Millim. Wave Technol. (ICMMT)*, May 2018, pp. 1–3.

[23] H. Li, B. Li, and L. Zhu, "A generalized synthesis technique for high-order and wideband 3-D frequency-selective structures with Chebyshev functions," *IEEE Trans. Antennas Propag.*, vol. 69, no. 7, pp. 3936–3944, Jul. 2021.

[24] H. Li, B. Li, and L. Zhu, "Wideband bandpass frequency-selective structures on stacked slotline resonators: Proposal and synthetic design," *IEEE Trans. Antennas Propag.*, vol. 68, no. 10, pp. 7068–7078, Oct. 2020.

[25] B. Li and Z. Shen, "Three-dimensional dual-polarized frequency selective structure with wide out-of-band rejection," *IEEE Trans. Antennas Propag.*, vol. 62, no. 1, pp. 130–137, Jan. 2014.

[26] G. Q. Luo, W. Hong, H. J. Tang, and K. Wu, "High performance frequency selective surface using cascading substrate integrated waveguide cavities," *IEEE Microw. Wireless Compon. Lett.*, vol. 16, no. 12, pp. 648–650, Dec. 2006.

[27] G. Q. Luo et al., "Theory and experiment of novel frequency selective surface based on substrate integrated waveguide technology," *IEEE Trans. Antennas Propag.*, vol. 53, no. 12, pp. 4035–4043, Dec. 2005.
[28] G. Q. Luo, W. Hong, Q. H. Lai, K. Wu, and L. L. Sun, "Design and experimental verification of compact frequency-selective surface with quasi-elliptic bandpass response," *IEEE Trans. Microw. Theory Techn.*, vol. 55, no. 12, pp. 2481–2487, Dec. 2007.
[29] G.-W. Chen et al., "High roll-off frequency selective surface with quasi-elliptic bandpass response," *IEEE Trans. Antennas Propag.*, vol. 69, no. 9, pp. 5740–5749, Sep. 2021.
[30] A. Abbaspour-Tamijani, K. Sarabandi, and G. M. Rebeiz, "Antenna-filter-antenna arrays as a class of bandpass frequency-selective surfaces," *IEEE Trans. Microw. Theory Techn.*, vol. 52, no. 8, pp. 1781–1789, Aug. 2004.
[31] S. Zheng, Y. Yin, J. Fan, X. Yang, B. Li, and W. Liu, "Analysis of miniature frequency selective surfaces based on fractal antenna-filter-antenna arrays," *IEEE Antennas Wireless Propag. Lett.*, vol. 11, pp. 240–243, 2012.
[32] Y. Li, L. Li, Y. Zhang, and C. Zhao, "Design and synthesis of multilayer frequency selective surface based on antenna-filter-antenna using Minkowski fractal structures," *IEEE Trans. Antennas Propag.*, vol. 63, no. 1, pp. 133–141, Jan. 2015.
[33] Y. Li et al., "Frequency selective surface with quasi-elliptic bandpass response using radiation null of patch antenna," *IEEE Antennas Wireless Propag. Lett.*, vol. 20, no. 1, pp. 13–17, Jan. 2021.
[34] H. Lin, Y. Li, S.-W. Wong, K. W. Tam, B. Liu, and L. Zhu, "High-selectivity FA-FA-based frequency selective surfaces using magnetoelectronic dipole antennas," *IEEE Trans. Antennas Propag.*, vol. 70, no. 11, pp. 10669–10677, Nov. 2022.
[35] G. Zhang, L. Ge, J. Wang, and J. Yang, "Design of a 3-D integrated wideband filtering magneto-electric dipole antenna," *IEEE Access*, vol. 7, pp. 4735–4740, 2018.
[36] K.-M. Luk and H. Wong, "A new wideband unidirectional antenna element," *Int. J. Microw. Opt. Technol.*, vol. 1, no. 1, pp. 35–44, Jun. 2006.
[37] B. Q. Wu and K. M. Luk, "A broadband dual-polarized magneto-electric dipole antenna with simple feeds," *IEEE Antennas Wireless Propag. Lett.*, vol. 8, pp. 60–63, 2008.
[38] L. Ge and K.-M. Luk, "A low-profile magneto-electric dipole antenna," *IEEE Trans. Antennas Propag.*, vol. 60, no. 4, pp. 1684–1689, Apr. 2012.
[39] M. Li and K. Luk, "A differential-fed magneto-electric dipole antenna for UWB applications," *IEEE Trans. Antennas Propag.*, vol. 61, no. 1, pp. 92–99, Jan. 2013.
[40] H. W. Lai, K. K. So, H. Wong, C. H. Chan, and K. M. Luk, "Magnetoelectric dipole antennas with dual open-ended slot excitation," *IEEE Trans. Antennas Propag.*, vol. 64, no. 8, pp. 3338–3346, Aug. 2016.
[41] L. Zhu, S. Sun, and W. Menzel, "Ultra-wideband (UWB) bandpass filters using multiple-mode resonator," *IEEE Microw. Wireless Compon. Lett.*, vol. 15, no. 11, pp. 796–798, Nov. 2005.
[42] S. W. Wong and L. Zhu, "Quadruple-mode UWB bandpass filter with improved out-of-band rejection," *IEEE Microw. Wireless Compon. Lett.*, vol. 19, no. 3, pp. 152–154, Mar. 2009.
[43] D. M. Pozar, *Microwave Engineering*. Boston, MA, USA: Artech House, 1998.

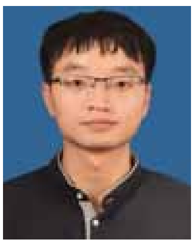

Huawei Lin received the B.S. degree in optoelectronic information science and engineering and the M.Eng. degree in electromagnetic field and microwave technology from Shenzhen University, Shenzhen, China, in 2017 and 2020, respectively. He is currently pursuing the Ph.D. degree in electrical and computer engineering with the University of Macau, Macau, China.

From July 2020 to March 2021, he was an Antenna Engineer with Shenzhen Sunway Communication Company Ltd., Shenzhen. From March 2021 to August 2021, he was a Research Assistant with the College of Electronics and Information Engineering, Shenzhen University. His research interests include antennas, decoupling techniques for MIMO antennas, RFID systems, and frequency-selective surfaces.

Sai-Wai Wong (Senior Member, IEEE) received the B.S. degree in electronic engineering from The Hong Kong University of Science and Technology, Hong Kong, in 2003, and the M.Sc. and Ph.D. degrees in communication engineering from Nanyang Technological University, Singapore, in 2006 and 2009, respectively.

From July 2003 to July 2005, he was an Electronic Engineer to lead the Electronic Engineering Department in China with two Hong Kong manufacturing companies. From May 2009 to October 2010, he was a Research Fellow with the Agency for Science,Technology and Research (ASTAR) Institute for Infocomm Research, Singapore. Since 2010, he has been an Associate Professor and later become a Full Professor with the School of Electronic and Information Engineering, South China University of Technology, Guangzhou, China. From July 2016 to September 2016, he was a Visiting Professor with the City University of Hong Kong, Hong Kong. Since 2017, he has been a Full Professor with the College of Electronics and Information Engineering, Shenzhen University, Shenzhen, China. He has authored or coauthored more than 200 articles in international journals and conference proceedings. His current research interests include RF/microwave circuit and antenna design.

Dr. Wong was a recipient of the New Century Excellent Talents in University awarded by the Ministry of Education of China in 2013 and the Shenzhen Overseas High-Caliber Personnel Level C in 2018.

Kam-Weng Tam (Senior Member, IEEE) received the B.Sc. degree in electrical and electronics engineering from the University of Macau, Macau, China, in 1993, and the joint Ph.D. degree in electrical and electronics engineering from the University of Macau and the Instituto Superior Tecnico, Technical University of Lisbon, Lisbon, Portugal, in 2000.

From 1993 to 1996, he was with the Instituto de Engenharia de Sistemas e Computadores (INESC), Lisbon, where he participated in research and development on a broad range of applied microwave technologies for satellite communication systems. From 2000 to 2001, he was the Director of INESC. In 2001, he cofounded the Microelectronic Design House Chipidea Microelectronica, Macau, where he was the General Manager until 2003. Since 1996, he has been with the University of Macau. He has authored or coauthored over 100 journal articles and conference papers. His current research interests include concerned multifunctional microwave circuits, RFID, UWB for material analysis, and terahertz technology.

Dr. Tam was a member of the organizing committees of 21 international and local conferences, including the Co-Chair of the 2008 Asia–Pacific Microwave Conference and the Technical Program, the IEEE MTT-S International Microwave Workshop Series on Art of Miniaturizing RF and Microwave Passive Components in 2008, and the 2010 International Symposium on Antennas and Propagation. He was an Interim Secretary for the establishment of the Macau Section in 2003. He supervised two IEEE Microwave Theory and Techniques Society (IEEE MTT-S) Undergraduate Scholarship recipients in 2002 and 2003. He was the Founder of the IEEE Macau AP/MTT Joint Chapter in 2010 where he was the Chair from 2011 to 2012.

Yin Li received the B.S. degree in applied physics from the China University of Petroleum, Dongying, China, in 2009, the M.Eng. degree in electromagnetic field and microwave technology from the University of Electronic Science and Technology of China (UESTC), Chengdu, China, in 2012, and the Ph.D. degree from the University of Macau, Macau, China.

From 2013 to 2015, he was a Research Assistant with The University of Hong Kong (HKU), Hong Kong, China. From 2019 to 2021, he was a Post-Doctoral Research Fellow with the College of Electronics and Information Engineering, Shenzhen University, Shenzhen, China. He is currently an Assistant Research Fellow with the Peng Cheng Laboratory, Shenzhen. His current research interests include numerical modeling methods of passive microwave circuits, computational electromagnetics, microwave circuits, frequency selectivity surface, and filtering antenna.

Kong Ngai received the double degrees in microelectronics technology and industrial electrical automation from the South China University of Technology, Guangzhou, China, in 1997, and the master's degree in electrical and electronic engineering from the University of Macau, Macau, China, in 2000.

He has been concerned about developing and applying wireless identification systems (RFID) for a long time. He is the Managing Director of Crosstech Innovation Group Limited, Macau, SAR, China. His current research interests include multifunctional microwave circuits, antennas, and RFID systems.

Mr. Ngai is currently the Vice Chairperson of the IEEE RFID Committee Macau Branch, China.

Chi-Hou Chio (Member, IEEE) received the B.Sc. degree in electrical and computer engineering from The University of Arizona, Tucson, AZ, USA, in 2009, and the M.Sc. degree in electrical and computer engineering from the University of Macau, Macau, China, in 2014, where he is currently pursuing the Ph.D. degree.

His current research interests include multifunctional microwave circuits and RFID systems.

Yejun He (Senior Member, IEEE) received the Ph.D. degree in information and communication engineering from the Huazhong University of Science and Technology (HUST), Wuhan, China, in 2005.

From 2005 to 2006, he was a Research Associate with the Department of Electronic and Information Engineering, The Hong Kong Polytechnic University, Hong Kong. From 2006 to 2007, he was a Research Associate with the Department of Electronic Engineering, Faculty of Engineering, The Chinese University of Hong Kong, Hong Kong. In 2012, he joined the Department of Electrical and Computer Engineering, University of Waterloo, Waterloo, ON, Canada, as a Visiting Professor. From 2013 to 2015, he was an Advanced Visiting Scholar (Visiting Professor) with the School of Electrical and Computer Engineering, Georgia Institute of Technology, Atlanta, GA, USA. Since 2011, he has been a Full Professor with the College of Electronics and Information Engineering, Shenzhen University, Shenzhen, China, where he is currently the Director of the Guangdong Engineering Research Center of Base Station Antennas and Propagation and the Director of the Shenzhen Key Laboratory of Antennas and Propagation. He has authored or coauthored over 260 referred journals and conference papers, and seven books. He holds about 20 patents. His research interests include wireless communications, antennas, and radio frequency.

Dr. He is a fellow of IET and a Senior Member of the China Institute of Communications and the China Institute of Electronics. He received the Shenzhen Science and Technology Progress Award in 2017 and has earned the Guangdong Provincial Science and Technology Progress Award for two times in 2018 and 2023. He earned the IEEE APS Outstanding Chapter Award in 2022. He was a recipient of the Shenzhen Overseas High-Caliber Personnel Level B ("Peacock Plan Award" B) and Shenzhen High-Level Professional Talent (Local Leading Talent). He is the Chair of the IEEE Antennas and Propagation Society-Shenzhen Chapter. He was selected as a Pengcheng Scholar Distinguished Professor, Shenzhen, and a Minjiang Scholar Chair Professor of Fujian Province, China, in 2020 and 2022, respectively. He has served as a Technical Program Committee Member or a Session Chair for various conferences, including the IEEE Global Telecommunications Conference (GLOBECOM), the IEEE International Conference on Communications (ICC), the IEEE Wireless Communication Networking Conference (WCNC), APCAP, EUCAP, UCMMT, and the IEEE Vehicular Technology Conference (VTC). He served as the TPC Chair for IEEE ComComAp 2021 and the General Chair for IEEE ComComAp 2019. He was selected as a Board Member of the IEEE Wireless and Optical Communications Conference (WOCC). He is serving as the TPC Co-Chair for WOCC 2023/2022/2019/2015. He acted as the Publicity Chair of several international conferences such as the IEEE PIMRC 2012. He is the Principal Investigator for over 30 current or finished research projects, including the National Natural Science Foundation of China, the Science and Technology Program of Guangdong Province and the Science and Technology Program of Shenzhen City. He has served as a Reviewer for various journals, such as the IEEE TRANSACTIONS ON VEHICULAR TECHNOLOGY, the IEEE TRANSACTIONS ON COMMUNICATIONS, the IEEE TRANSACTIONS ON INDUSTRIAL ELECTRONICS, the IEEE TRANSACTIONS ON ANTENNAS AND PROPAGATION, the IEEE WIRELESS COMMUNICATIONS, the IEEE COMMUNICATIONS LETTERS, the *International Journal of Communication Systems*, *Wireless Communications and Mobile Computing*, and *Wireless Personal Communications*. He is serving as an Associate Editor for IEEE TRANSACTIONS ON ANTENNAS AND PROPAGATION, IEEE TRANSACTIONS ON MOBILE COMPUTING, *IEEE Antennas and Propagation Magazine*, IEEE ANTENNAS AND WIRELESS PROPAGATION LETTERS, *International Journal of Communication Systems*, and *China Communications*. He served as an Associate Editor for *IEEE Network*.